Decision-Feedback Equalization of Bandwidth-Constrained N-WDM Coherent Optical Communication Systems

Jessica Fickers[1], Amirhossein Ghazisaeidi[2], Massimiliano Salsi[2], Gabriel Charlet[2], Philippe Emplit[1], François Horlin[1],
[1]OPERA Department, Université libre de Bruxelles, jfickers@ulb.ac.be
[2]Alcatel-Lucent Bell Labs, Centre de Villarceaux, Nozay, France

***Abstract*—Nyquist Wavelength division multiplexing (N-WDM), is a promising scheme in order to enhance the spectral efficiency of future coherent optical communication systems. In N-WDM systems, the channel bandwidth and spacing are selected to maximize the spectral efficiency while maintaining acceptable levels of inter-carrier and inter symbol interference. To further increase the spectral efficiency, bandwidth constrained N-WDM, where baudrate is higher than channel bandwidth can be considered. We propose to combine the bandwidth-constrained N-WDM scheme with a decision feedback equalizer (DFE) designed according to the minimum mean square error (MMSE) criterion. We show that the enhanced resilience to the inter symbol interference offered by DFE provides an effective gain on spectral efficiency. We compare system benefits of DFE and maximum a posteriori sequence detection (MAP) for coherent optical receivers, and show that DFE is as efficient as MAP in mitigating inter symbol interference at a considerably lower complexity.**

I. Introduction

In wavelength division multiplexed (WDM) optical communication systems, increasing the spectral efficiency (SE) is essential in order to reach higher capacity targets. High SE can be achieved by using either high-order modulation formats and/or reduced channel spacing. When the channel spacing is reduced, the communication channels suffer from inter-channel interference (ICI); substantial effort is currently devoted to optimize pulse shaping for high-SE systems with tight channel packing [1].

In conventional WDM systems using the 50 GHz ITU grid and without pulse shaping [2]–[4], the 10-dB bandwidth of the WDM channel is typically higher than the symbol rate. A promising solution for WDM systems using pulse shaping at the transmitter is Nyquist-WDM (N-WDM). N-WDM systems operate with pulses with sinc temporal profile and rectangular spectrum, therefore the bandwidth of the channels is equal to the symbol rate, and very high SE can be achieved at zero inter symbol interference (ISI). The stringent constraints for the generation of N-WDM require new techniques for the implementation of pulse shaping. The digital symbols can be pre-shaped into nearly rectangular spectra and then converted to analog waveforms using high-speed digital to analog converters (DAC) [5]–[7].

Lately, a substantial research effort has been put into the development of sub-baudrate-spaced channels, where the bandwidth of the pulse shaping filters is decreased below the symbol rate to avoid linear crosstalk [8], [9]. In this scenario, the per-channel bandwidth constraint dramatically increases ISI, so powerful ISI equalization techniques should be employed [8], [10]. Another scenario in which ISI dominates is where WDM channels are narrowly filtered due to multiple cascaded reconfigurable optical add-drop multiplexers (ROADM) [11] .

In polarization division multiplexed (PDM) optical coherent receivers, ISI and ICI are partly equalized by the polarization demultiplexing digital signal processing (DSP) block, consisting of four butterfly-structured feedforward (FF) finite impulse response (FIR) filters that are adaptively updated using, for example, the constant modulus algorithm (CMA) [12]. However, in N-WDM, the ISI mitigation offered by the polarization demultiplexing DSP block is not sufficient. This is expected, since CMA-FF equalizer performance is comparable to linear equalizers [13], and it is known that linear equalizers perform poorly given strong channel selectivity [14].

Some authors have proposed to use a direct implementation of maximum a posteriori (MAP) sequence detection to combat ISI in tightly-filtered PDM-WDM transmission systems, and demonstrated substantial equalization gain over CMA-FF equalizer [9], [15]. A direct implementation employs a look-up table of all possible sequences of N_{MAP} consecutive transmitted symbols, where N_{MAP} is the equalizer memory. The complexity of this detection scheme grows thus exponentially with N_{MAP}.

Decision feedback equalizers (DFE) have been proposed for chromatic dispersion compensation [16] as well as carrier phase estimation [17] in single carrier coherent optical communications. In [18], the authors propose a DFE to enhance the tolerance of digital signal processing to phase noise.

In this paper we propose to use DFE to mitigate ISI in bandwidth-constrained N-WDM. The ISI mitigation offered by DFE is superior to linear equalizers while its complexity remains manageable compared to MAP. The interaction between CMA-FF and DFE is studied, and the performance/complexity trade-off of DFE and MAP is addressed. The structure of the paper is as follows: in Section II we detail the equalizer

structure. Numerical results are presented in Sections III, and conclusions are drawn in Section IV.

II. Equalizer structure

It is now standard to use the CMA-FF to demultiplex polarizations and perform per-channel equalization of residual dispersion and polarization mode dispersion to some extent. As is the usual practice we suppose the signal is sampled at two samples per symbol at CMA-FF input and is down-sampled to one sample per symbol at CMA-FF output, and followed by a MMSE-DFE designed to further mitigate ISI.

The MMSE-DFE makes use of both the received sequence (feedforward section, MMSE-FF) and the previously detected symbols (feedback section, MMSE-FB) to remove the interference they cause on the currently estimated symbol. The filter taps of the MMSE-FF and MMSE-FB sections are derived based on MMSE criterion. The details can be found in [19]. In our implementation, the calculation of the equalizer filter coefficients requires the use of a known training sequence on each polarization separately which is legitimate since the CMA compensates for the polarization impairments.

Let us denote the transmitted training sequence symbols by $x[\cdot]$, and their estimation at the output of MMSE-FF by $\hat{x}[\cdot]$. The estimation error is $\epsilon[i] = x[i] - \hat{x}[i]$, for $i = 1, ..., M$, where M is the training sequence length. The training sequence is constructed by l times repeating a training pattern of length N; therefore $M = lN$. We should have $N > N_{\text{eff}}$, where N_{eff} is channel effective memory. Under this condition the continuous-time equalizer can be derived from the burst-mode matrix model [20]. The details of derivations are given in [19]. In the following we quote the main results.

Let the error vector calculated over k-th burst ($k = 1, ..., l$) inside the training sequence be denoted by $\underline{\epsilon}_k$. It is explicitly written as

$$\underline{\epsilon}_k = [\epsilon[(k-1)N+1], ..., \epsilon[kN]]^T \tag{1}$$

where superscript T stands for matrix transpose. The $N \times N$ error autocorrelation matrix is denoted by $\underline{\underline{R}}$ and calculated as

$$\underline{\underline{R}} = \frac{1}{l}\sum_{j=1}^{l} \underline{\epsilon}_j \underline{\epsilon}_j^H \tag{2}$$

where superscript H stands for Hermitian conjugation. Next we calculate the LDU decomposition [21] of the positive definite and symmetric $\underline{\underline{R}}$ as follows

$$\underline{\underline{R}} = \underline{\underline{P}}\, \underline{\underline{\Lambda}}\, \underline{\underline{P}}^H \tag{3}$$

where $\underline{\underline{\Lambda}}$ is a diagonal matrix and $\underline{\underline{P}}$ is an upper triangular matrix. The impulse response of MMSE-FF, and MMSE-FB parts of the DFE are denoted by $h_f[\cdot]$ and $h_b[\cdot]$ respectively, and are given by the following equations

$$h_f[i] = A_{N/2, N/2-i} \tag{4}$$

$$h_b[i] = h_f[i+1] \tag{5}$$

where $\underline{\underline{A}} \doteq \underline{\underline{P}}^{-1}$, and $A_{m,n}$ is the element of $\underline{\underline{A}}$ found on row m and column n. In (5), $i = 0, ..., N/2-1$ in (4) and $i = 0, ..., N/2-2$.

It is important to stress that the impulse responses $h_f[\cdot]$ and $h_b[\cdot]$, are derived based on the training sequence only. During transmission of the payload, the MMSE-DFE is not updated unlike the CMA-FF. The MMSE-DFE is designed to mitigate ISI stemming from the bandwidth constraint which is constant in time. In Sections III, we prove that MMSE-DFE is compatible with the standard DSP for channel tracking in PDM-quaternary phase shift keying systems. One advantage of a training-based DFE derivation is that the stability of the equalizer is not impaired at high error rates. As a consequence, very high target BERs can be considered.

III. Numerical Results

A. Simulation setup

The simulation setup is illustrated in Figure 1. 2^{16} bits were generated by periodically repeating a pseudo random binary sequence (PRBS) of length $2^{15}-1$. The bits are mapped to quaternary phase shift keying (QPSK) symbols with one sample per symbol. These sequences are then upsampled by a factor of two and digitally shaped using a time-domain root-raised-cosine (RRC) FIR filter with a rolloff factor equal to 0.05. The symbol rate is constant and equal to 32 Gbaud. The digital bandwidth Ω is defined as the 3-dB bandwidth of the RRC-FIR filter. It is varied between 27.2 and 32 Gbaud for a constant symbol rate of $B = 32$ Gbaud. When the digital bandwidth is equal to 32 Gbaud, no ISI is present provided that the receiver RRC filter is matched to the transmitter. Three channels are simulated and the BER is assessed on the central channel. The channel spacing is varied to allow for different values of spectral efficiency. The signals are digital to analog converted using DACs and passed to the electrical driver. They are modulated by an IQ modulator (IQM) with a linear transfer function and multiplexed by a 3×1 coupler. Moreover, the bandwidth limitations of the DACs and the electrical driver are neglected. A sinc impulse response was used to simulate the combined DAC + anti-aliasing filter. The amplified spontaneous emission (ASE) is assumed additive white Gaussian noise. At the receiver, the signals go through the coherent mixer. The signals are sampled at two samples per symbol by analog-to-digital convertors (ADC). The electrical front-end of the photodiodes and ADC are simulated as a 3^{rd}-order super Gaussian lowpass filter. The 3-dB bandwidth of the electrical front-end is set to 32 GHz. The digital signals are equalized as explained in Section II, using a combination of CMA and MMSE-DFE. To detect the signals, we performed MAP sequence detection for comparative results in Section III-E, or standard symbol-by-symbol minimum distance detection for the rest. The BER is estimated by Monte Carlo simulations, where the noise seed is randomly varied. In addition, the relative delay and polarization of neighboring channels are randomly varied. We count at least 500 errors, and convert the bit error rate into the Q^2- factor:

$$Q^2 = 20\log_{10}\left(\sqrt{2}\text{erfc}^{-1}(2\text{BER})\right) \tag{6}$$

where erfc^{-1} is the inverse complementary error function and Q^2 is in dB. In the following sections, we assume zero carrier

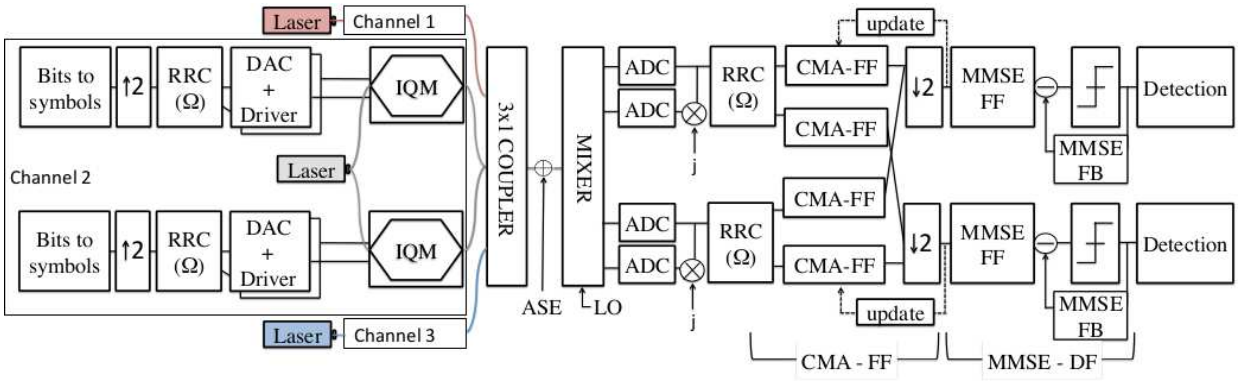

Fig. 1. The simulation setup, QPSK: quaternary phase shift keying, DAC: digital-to-analog conversion, IQM: IQ-modulator, ADC: analog-to-digital conversion, CMA: constant modulus algorithm, ASE: amplified spontaneous emission, LO: local oscillator, MMSE-FF : feedforward filter of the MMSE-DFE, MMSE-FB: feedback filter of the MMSE-DFE. $j = \sqrt{-1}$. The symbol rate B is constant and $= 32$ Gbaud while the RRC-FIR digital bandwidth is equal to $\Omega \leq 32$ GHz.

frequency offset between the carrier and the local oscillator and carrier phase noise, and polarization alignment between the central channel and the local oscillator. In Section III-F, we study the resilience of the MMSE-DFE to laser phase noise. In the following sections, we assess the performance of the N-WDM system using per-channel MMSE-DFE.

B. Simulation parametrization

In this subsection, we specify how we chose the pulse shaping finite impulse response (FIR) filter length N_{FIR}, CMA filter length N_{CMA} and digital bandwidth Ω. The reference bandwidth for the OSNR is 0.1 nm and the OSNR is subsequently noted $\mathrm{OSNR}_{(0.1\ nm)}$.

In Fig. 2(a), we investigate the required pulse shaping length for the bandwidth-constrained N-WDM systems. The number of taps of the RRC-FIR pulse shaping filter is varied. We simulate the non-constrained case $N_{\mathrm{FIR}} = \infty$ by applying the shaping filter in the frequency domain on the whole signal vector. In all other cases, the signal vector is convolved with the truncated impulse response of the pulse shaper in the time domain. We conclude that $N_{\mathrm{FIR}} = 64$ is sufficient to achieve a performance similar to the non-constrained case, whereas a $\mathrm{OSNR}_{(0.1\ nm)}$ penalty of about 0.5 dB appears when N_{FIR} is as small as 16. In the rest of the results, $N_{\mathrm{FIR}} = 64$.

In Fig. 2(b), we study the impact of the CMA-FFs of various lengths N_{CMA} prior to the MMSE-DFE. System performance at various channel spacings is shown vs. N_{CMA} ranging from 0 to 13. The $N_{\mathrm{CMA}} = 0$ represents the case where no CMA-FF is used. Note that in reality, using CMA-FF is obligatory to retrieve the polarization axes; however, in the numerical studies presented in this paper, we are only interested in the equalization characteristics of CMA-FF and DFE blocks; therefore, in all the simulations the polarization axes at TX and RX are aligned. Comparing system performance at $N_{\mathrm{CMA}} = 0$ and larger value of N_{CMA} we conclude that the DFE does not benefit from prior CMA-FF. Moreover, increasing N_{CMA} beyond 13 did not influence Q^2 so the results were not reported. We conclude that regardless of N_{CMA}, the CMA-FF does not have significant influence on the performance of the bandwidth-constrained N-WDM system with small rolloff. Paper [22] showed that the polarization tracking ability of the CMA-FF can be generalized to bandwidth-constrained systems. As a consequence, the generated results regarding the MMSE-DFE without CMA-FF can be directly generalized to transmission schemes using CMA-FF. In particular, links with time-variant polarization impairments, which are taken care of by the CMA-FF, can be studied. This paper concentrates on back-to-back simulations only. In the case of uncompensated long-haul transmission, the CMA-FF is generally used to remove any residual chromatic dispersion and polarization mode dispersion from the signal. Even without CMA-FF, the MMSE-DFE should mitigate residual chromatic dispersion if the number of channel memory taps stemming from this impairment does not exceed the number of taps of the MMSE-DFE. However, polarization mode dispersion cannot be mitigated by our MMSE-DFE because it is implemented per-polarization. As a conclusion, for long-haul transmission, in opposition to the back-to-back case illustrated here, the CMA-FF would have a significant impact on the system performance because of cross-polarization effects.

In Fig.2(c), we assess the influence of the digital bandwidth. When the channel spacing decreases, the system is limited by ICI besides the ISI. A trade-off exists between the two sources of interference. With decreasing Ω, ICI limitations become less stringent as the channel bandwidth decreases, but ISI is created. In Fig. 2(c) the optimum can be observed. For each channel spacing where ISI is preset, the optimum performance is achieved when $\Omega \approx \Delta f$.

In Fig. 3, we study the influence of the overall length of the training sequence M on system performance. Since the MMSE-DFE FF and FB filters are derived only once at the beginning of the transmission, they do not generate a large overhead. Nonetheless, it is interesting to evaluate the minimum length of the training sequence to assure a satisfactory estimation of the autocorrelation matrix $\underline{\underline{R}}$. Fig. 3 shows that the performance saturates at $M \approx 1000$ symbols.

C. Parametrization of MMSE-DFE

In the following results, we assess the performance of the MMSE-DFE with respect to its memory depth L. In this

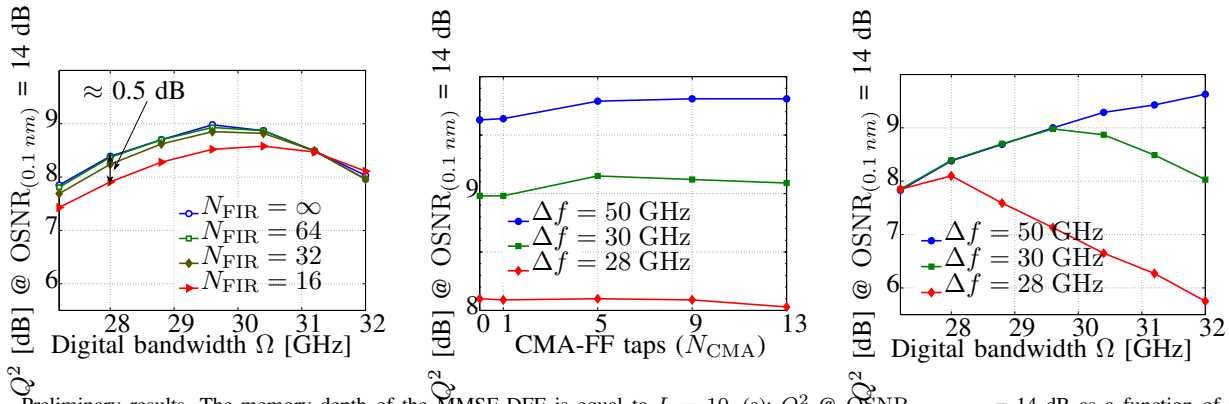

Fig. 2. Preliminary results. The memory depth of the MMSE-DFE is equal to $L = 10$. (a): Q^2 @ OSNR$_{(0.1\ nm)}$ = 14 dB as a function of the digital bandwidth for different numbers of RRC-FIR taps. The CMA-FF is not used.The channel spacing is equal to 30 GHz. (b): Q^2 @ OSNR$_{(0.1\ nm)}$ = 14 dB as a function of the memory of the CMA-FF (N_{CMA}). $N_{\mathrm{FIR}} = 64$. The digital bandwidth is equal to the channel spacing. (c): Q^2 @ OSNR$_{(0.1\ nm)}$ = 14 dB as a function of the digital bandwidth for three different channel spacings. The CMA-FF is not used. $N_{\mathrm{FIR}} = 64$.

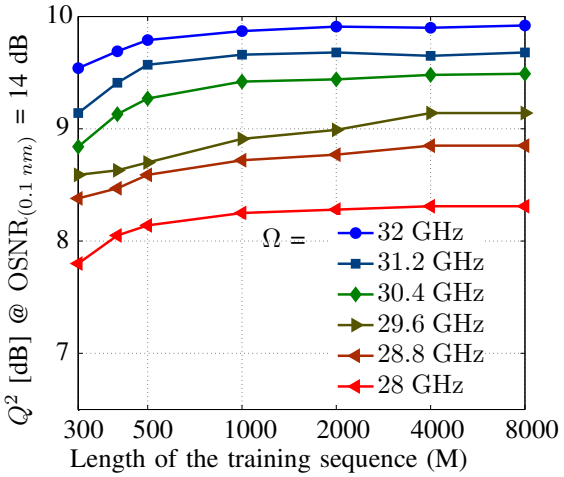

Fig. 3. Preliminary results. System performance as a function of the length of the training sequence. The CMA-FF equalizer is not used. The number of RRC-FIR taps of the pulse shaping filter $N_{\mathrm{FIR}} = 64$. The memory depth of the MMSE-DFE is equal to $L = 10$.

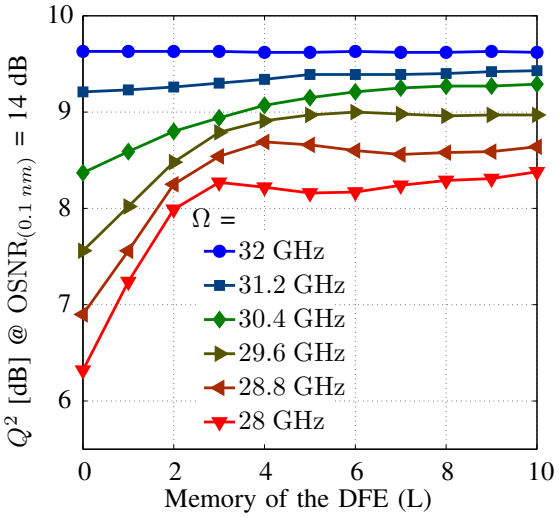

(a) Q^2 @ OSNR$_{(0.1\ nm)}$ = 14 dB. $\Delta f = 50$ GHz

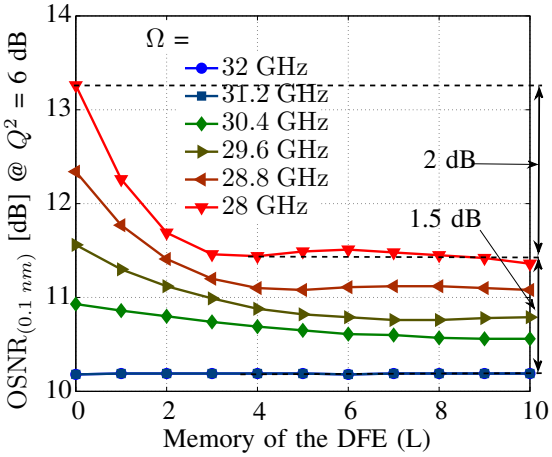

(b) OSNR$_{(0.1\ nm)}$ @ Q^2 = 6 dB. $\Delta f = 50$ GHz

Fig. 4. System performance as a function of the MMSE-DFE memory depth. $\Delta f = 50$ GHz. The CMA-FF equalizer is not used. The number of RRC-FIR taps of the pulse shaping filter $N_{\mathrm{FIR}} = 64$.

section, only the performance of the MMSE-DFE is assessed. In Section III-D, the MMSE-DFE is combined with linear equalizers. In Figure 4, we study the performance of the DFE when the channel spacing $\Delta f = 50$ GHz. No ICI is present since the channel spacing is much larger than the channel bandwidth. Both the Q^2 for a fixed OSNR$_{(0.1\ nm)}$ of 14 dB and the OSNR$_{(0.1\ nm)}$ at a fixed target of $Q^2 = 6$ dB are presented. The results are shown as a function of the number of MMSE-FB taps L. When $L = 0$, there is no feedback (MMSE-FB) and the feedforward section (MMSE-FF) contains only one tap equal to 1. When L increases, the FB loop takes into account more and more past decisions. We therefore assess both the performance gain stemming from the use of the DFE and the number of taps required for its use. When the digital bandwidth is decreased, Q^2 is degraded. It can be seen that the MMSE-DFE offers a performance gain when the digital bandwidth is smaller than 30 GHz. When the digital bandwidth is equal to 28 GHz, the OSNR$_{(0.1\ nm)}$ to achieve Q^2 = 6 dB raises by 3.5 dB and thanks to the use of the MMSE-DFE, the penalty is reduced to 1.5 dB. However, there is still residual ISI. The performance is not further enhanced when L

is increased beyond 4 taps.

In Fig. 5, we assess the MMSE-DFE gain in the presence of ICI. In Fig. 5 the $\mathrm{OSNR}_{(0.1\ nm)}$ at Q^2 = 6 dB is shown as a function of the number of MMSE-DFE taps, for Δf = 30 GHz in Fig. 5(a) and 28 GHz in Fig. 5(b), respectively, for different digital bandwidths. Comparing Fig. 2(a) and 5, we can conclude that the optimum bandwidth is equal to the channel spacing regardless of the length of the MMSE-DFE.

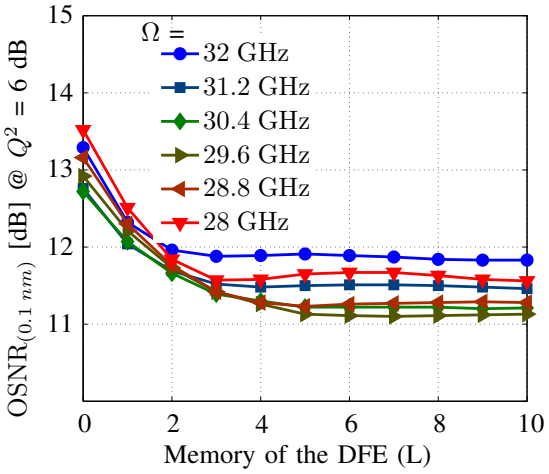

(a) $\mathrm{OSNR}_{(0.1\ nm)}$ @ Q^2 = 6 dB. $\Delta f = 30$ GHz

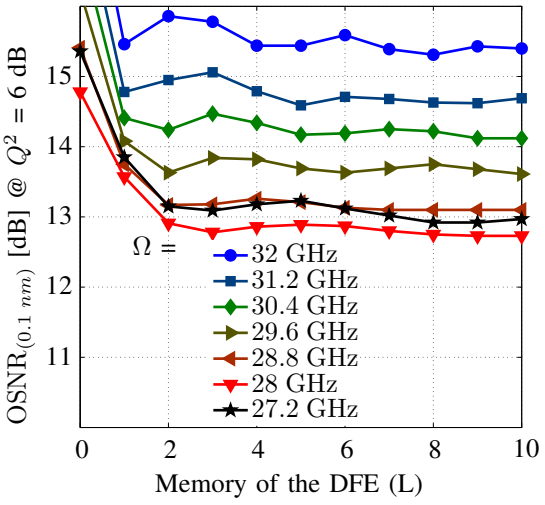

(b) $\mathrm{OSNR}_{(0.1\ nm)}$ @ Q^2 = 6 dB. $\Delta f = 28$ GHz

Fig. 5. System performance as a function of the MMSE-DF memory depth. The CMA-FF equalizer is not used. The number of RRC-FIR taps of the pulse shaping filter $N_{\mathrm{FIR}} = 64$.

D. Performance of MMSE-DFE

According to the results of the preceding sections, the simulation parameters are listed and the notations defined in Table I.

In Fig. 6, we show the performance of the combined CMA-FF ($N_{\mathrm{CMA}} = 13$ taps) and MMSE-DFE for an optimized digital bandwidth. The DFE performance gain can be observed,

TABLE I
SIMULATION PARAMETERS

Parameter	Symbol	Value range
Length of estimation bursts (bits)	N	50
Length of training sequence (bits)	M	8000
Channel spacing [GHz]	Δf	28 - 50
Digital bandwidth [GHz]	Ω	28-32
DFE memory depth	L	0-10
CMA taps	N_{CMA}	13
Number of taps of the pulse shaping RRC-FIR	N_{FIR}	64
Symbol rate [Gbaud]	B	32

keeping in mind that $L = 0$ corresponds to CMA-FF-only equalization. When Δf = 30 GHz, the $\mathrm{OSNR}_{(0.1\ nm)}$ @ Q^2 = 6 dB is 0.8 dB lower when using a MMSE-DFE with a sufficient number of taps, whereas the $\mathrm{OSNR}_{(0.1\ nm)}$ gain is as large as 2 dB for Δf = 28 GHz. In this case, the $\mathrm{OSNR}_{(0.1\ nm)}$ penalty with respect to the Δf = 50 GHz is as low as 1.5 dB, as already noted in Fig. 5 .

In Fig. 7, we extend our study to another linear equalizer, a cross-polarization linear equalizer based on the MMSE-criterion [14] implemented at one sample per symbol. Like the DFE, it is data-aided and based on channel estimation. Thanks to the training symbols, a two-input two-output channel matrix is derived, taking into account ISI as well as polarization effects. Using this matrix, the MMSE burst-mode equalizer is derived and extended to a continuous-time equalizer using the method presented in [20].

Different combinations of the three equalizers, i.e CMA-FF, linear MMSE and MMSE-DFE are studied. We note that the combination of CMA-FF and MMSE fails to mitigate the ISI stemming from tight filtering. CMA-FF and MMSE have a very similar performance for all channel spacings. Finally, as already noted in Fig. 2 for the special case of CMA-FF, the DFE does not benefit from prior linear equalization.

E. Comparison with MAP

In Fig. 8 and 9, we compare the performance of the MMSE-DFE with a direct implementation of the MAP-detector as in [15]. Similarly to the MMSE-DFE, the MAP detector operates separately on each polarization tributary. We present results for a MAP with $N_{\mathrm{MAP}} = 3$ taps and $N_{\mathrm{MAP}} = 5$ taps. The complexity of the equalizer becomes prohibitive beyond this value. In our simulations, we focused on PDM-QPSK. In a more general context, due to the number of entries of the MAP look-up-table, the complexity of the MAP detector is of $O(C^{N_{\mathrm{MAP}}})$, where C is the alphabet size. This makes it extremely difficult to implement MAP detection for higher order modulations [11], whereas the complexity of the MMSE-DFE is largely determined by the cost of LDU decomposition of the error autocorrelation matrix. This complexity is of $O(N^3)$ [21] and does not depend on the alphabet size. In a MAP equalizer with $N_{\mathrm{MAP}} = 3$, when detecting a given symbol, the interference from the preceding symbol and the following symbol are taken into account. On the contrary, for MMSE-DFE with a memory depth $L = 1$, only the preceding decision is fed into the feedback loop. It is however interesting to compare these equalizers at a given memory

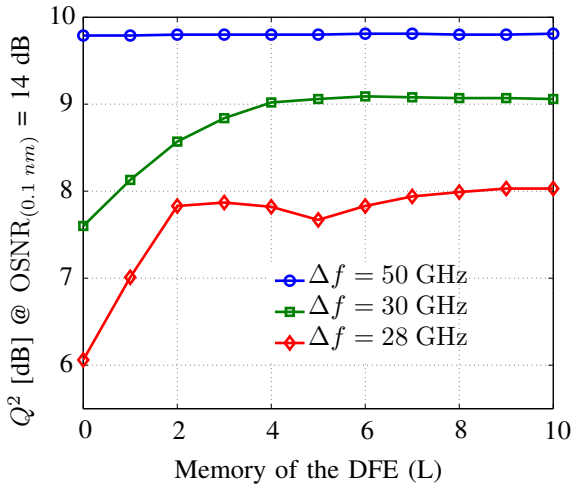

(a) Q^2 @ OSNR$_{(0.1\ nm)}$ = 14 dB

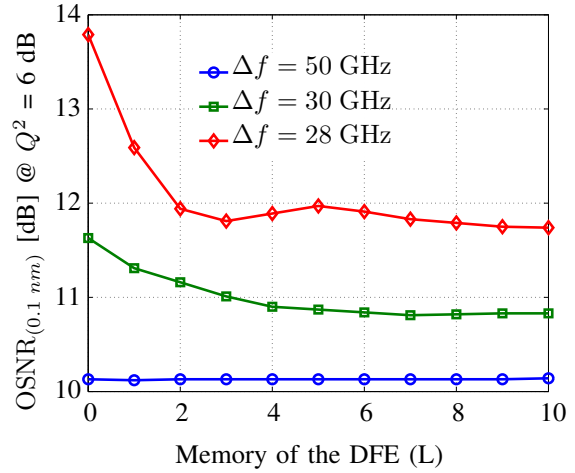

(b) OSNR$_{(0.1\ nm)}$ @ Q^2 = 6 dB

Fig. 6. System performance as a function of the MMSE-DF memory depth for three different channel spacings. The digital bandwidth is equal to the channel spacing. The number of taps of the CMA-FF $N_{\mathrm{CMA}} = 13$. The number of RRC-FIR taps of the pulse shaping filter $N_{\mathrm{FIR}} = 64$.

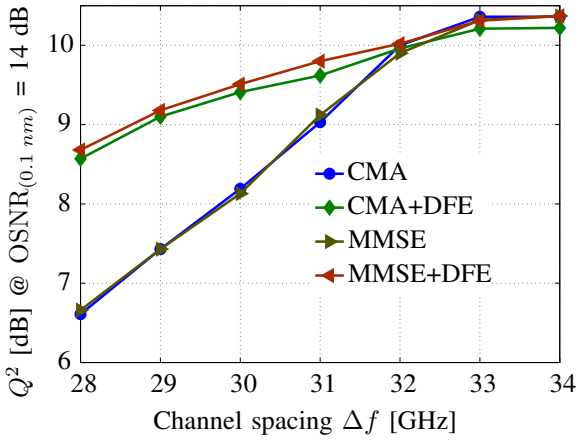

(a) Q^2 @ OSNR$_{(0.1\ nm)}$ = 14 dB.

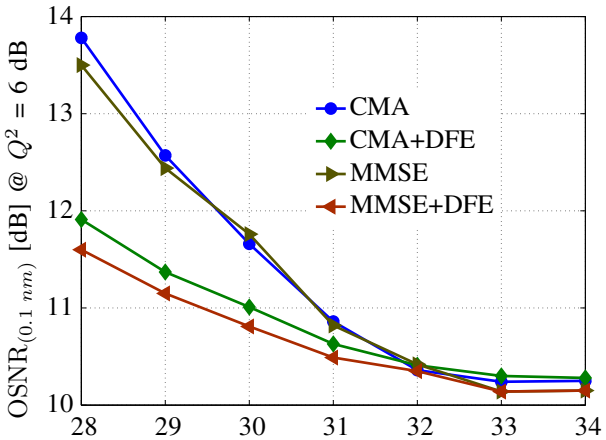

(b) OSNR$_{(0.1\ nm)}$ @ Q^2 = 6 dB.

Fig. 7. System performance as a function of the channel spacing for different equalizers. The number of FIR taps of the pulse shaping filter $N_{\mathrm{FIR}} = 64$. When used, the number of taps of the CMA-FF is $N_{\mathrm{CMA}} = 13$. The length of the MMSE equalizer was equal to 50 taps. When used, the memory depth of the DFE was equal to $L = 10$ taps. The digital bandwidth Ω was equal to the channel spacing.

depth, i.e.: $\mathrm{MAP}_{N=3}$ / $\mathrm{MMSE-DFE}_{L=1}$ and $\mathrm{MAP}_{N=5}$ / $\mathrm{MMSE-DFE}_{L=2}$. For $\mathrm{MAP}_{N=5}$, the number of entries in the MAP look-up-table is equal to $C^{N_{\mathrm{MAP}}} = 1024$. For each symbol, every entry is compared with a received sequence of length $N_{\mathrm{MAP}} = 5$, leading to a number of complex multiplications, additions and comparisons roughly (256×5) times higher than symbol-by-symbol detection. For $\mathrm{MMSE-DFE}_{L=4}$ which shows similar performance, the equalization merely consists of two convolutions by FIR filters of very short lengths $L+1$ and L respectively, subtraction and symbol-by-symbol decision. We only add ≈ 20 complex multiplications and additions and one subtraction per equalized symbol to the symbol-by-symbol detection complexity. Fig. 8 shows that the MAP equalizer generally performs better than MMSE-DFE at the same memory depth, the performance difference increasing with the bandwidth constraint. However with only one increment in memory depth, the MMSE-DFE performs similarly as the MAP equalizer for both $N_{\mathrm{MAP}} = 3$ and 5. This gives a clear advantage to the MMSE-DFE, because of its reduced complexity with respect to the MAP equalizer, at the cost of the presence of a feedback.

The performance of MMSE-DFE at high BER is illustrated in Fig. 9, where Q^2 is given as a function of OSNR$_{(0.1\ nm)}$ for $\mathrm{MMSE-DFE}_{L=4}$ and $\mathrm{MAP}_{N=5}$. Q^2 as low as 4 dB have been considered. It is to be noted that the MMSE-DFE performance does not degrade with respect to MAP for very low OSNR$_{(0.1\ nm)}$. We study the feedback error propagation of MMSE-DFE by adding the MMSE-DFE Q^2 when the feedback signal is forced to be the correct symbols. As already pointed out in Section II, thanks to training-based derivation, the MMSE-DFE does not suffer from catastrophic error propagation at high BER. The performance loss from

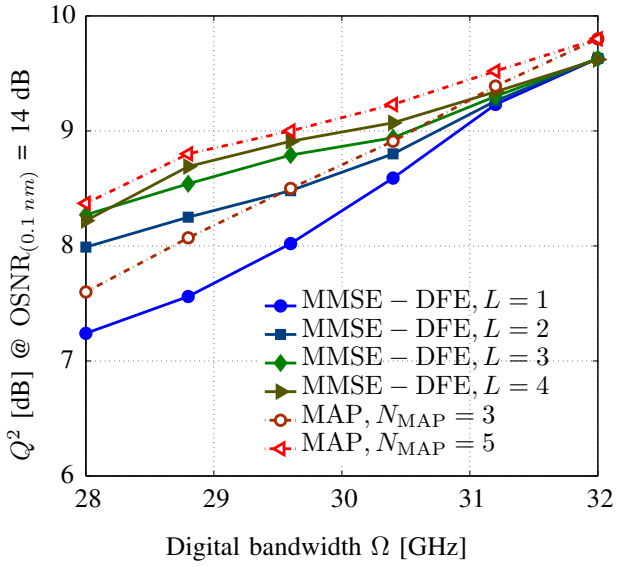

(a) Q^2 @ OSNR$_{(0.1\ nm)}$ = 14 dB

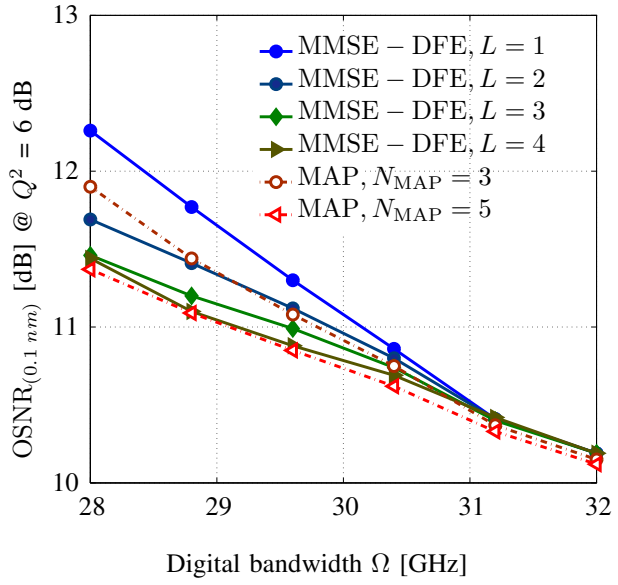

(b) OSNR$_{(0.1\ nm)}$ @ Q^2 = 6 dB

Fig. 8. System performance using MMSE-DFE or MAP inter symbol interference mitigation for different memory depths of the equalizers. The channel spacing is equal to 50 GHz. The CMA-FF equalizer is not used. The number of RRC-FIR taps of the pulse shaping filter $N_{\mathrm{FIR}} = 64$.

feedback error propagation does not exceed 0.6 dB even at a digital bandwidth of 28 GHz and OSNR$_{(0.1\ nm)}$ as low as 8 dB.

F. Resilience to phase noise

Here we study the impact of laser phase noise on the performance of the modulation scheme using the MMSE-DFE. We suppose an ideal local oscillator, thus laser phase noise is simulated for the transmitter laser only. Frequency dithering is ignored. The phase of the transmission laser is simulated

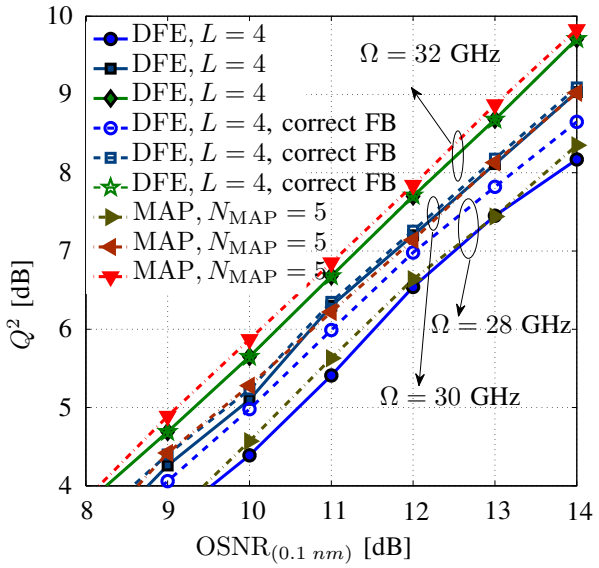

Fig. 9. System performance using MMSE-DFE or MAP inter symbol interference mitigation for different OSNR$_{(0.1\ nm)}$. The channel spacing is equal to 50 GHz. The CMA-FF equalizer is not used. The number of RRC-FIR taps of the pulse shaping filter $N_{\mathrm{FIR}} = 64$.

as a random walk whose step size is a zero mean Gaussian random variable, yielding the approximation of a Lorentzian laser line shape [23]. The laser phase noise is mitigated using the well-known Viterbi and Viterbi (V+V) algorithm [24] taking profit from the symmetry of the QPSK constellation. The sliding-window averaging length of the V+V is equal to 64 symbols through all simulations. Because of the $\pi/2$-ambiguity of the V+V detection, differentially encoded and decoded QPSK is implemented in this simulation. The V+V is applied after the CMA-FF and prior to the MMSE-DFE. Therefore, we investigate both the robustness of the V+V to bandwidth constraints and the robustness of the MMSE-DFE to residual phase noise and cycle slips. In Fig. 10, the channel spacing is fixed to 30 GHz. From Fig. 10, we conclude that the V+V is usable in the context of bandwidth-constrained PDM-QPSK transmission schemes for laser bandwidths up to 1 MHz. When the laser linewidth is equal to 500 kHz, the OSNR$_{(0.1\ nm)}$ penalty @ Q^2 = 6 dB is about 0.25 dB. This penalty does not depend on the number of DFE taps used. As a conclusion, the stability of the MMSE-DFE is not impaired by residual phase noise.

IV. Conclusion

In this paper, we assessed the effect of the use of MMSE-DFE in N-WDM coherent optical communication systems with sub-symbol rate channel bandwidth for high spectral efficiency. We studied the impact of the digital channel bandwidth on system performance and showed that the channel spacing should be approximately equal to the digital bandwidth. We further showed that the use of a MMSE-DFE greatly enhances the performance when the channel spacing is smaller than the symbol rate. For a channel baud rate of 32 Gbaud, the channel

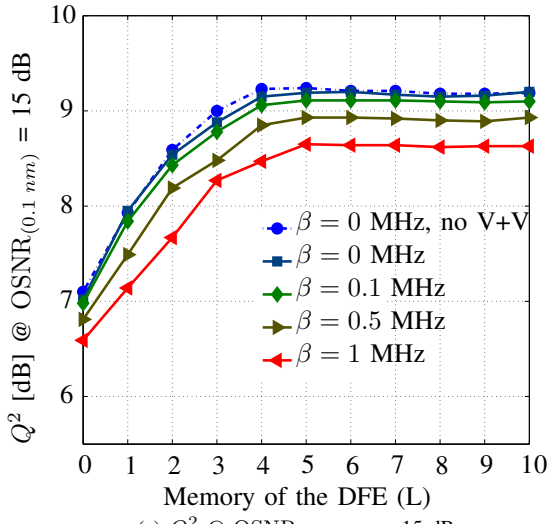

(a) Q^2 @ OSNR$_{(0.1\ nm)}$ = 15 dB

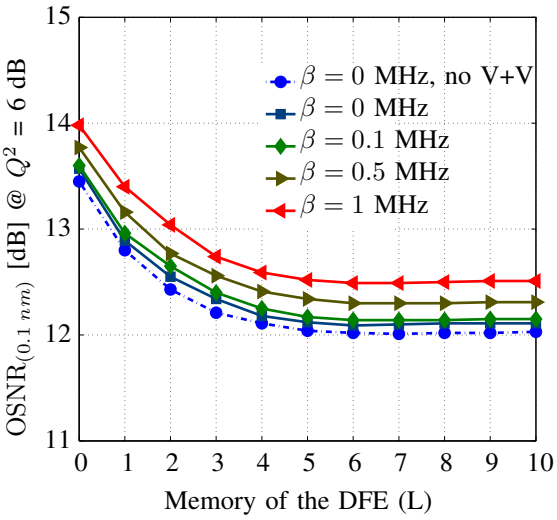

(b) OSNR$_{(0.1\ nm)}$ @ Q^2 = 6 dB

Fig. 10. System performance as a function of the number of MMSE-DFE taps. The channel spacing is equal to 30 GHz. The digital bandwidth is equal to the channel spacing. The CMA-FF is not used. The 3-dB transmission laser linewidth β is varied.

spacing could be decreased to 28 GHz thanks to the MMSE-DFE with a OSNR$_{(0.1\ nm)}$ penalty (at Q^2 = 6 dB) as low as 1.5 dB with respect to the single channel case. In this case, the OSNR$_{(0.1\ nm)}$ MMSE-DFE gain was as high as 2 dB. Thanks to the polarization tracking ability of the blind CMA-FF, our results can be generalized to links with time-variant polarization effects. We showed that when the memory length is carefully chosen, the MMSE-DFE with $L = 4$ performs similarly to a MAP detector with $N_{\mathrm{MAP}} = 5$, while offering a reduced computational complexity. Finally, we showed that the MMSE-DFE is robust to residual phase noise stemming from imperfect transmission lasers.

REFERENCES

[1] X. Zhou, L. Nelson, P. Magill, B. Zhu, and D. Peckham, "8x450-gb/s, 50-GHz-spaced, PDM-32QAM transmission over 400km and one 50GHz-grid ROADM," in *Proc. Opt. Fiber Comm. Conf. (OFC/NFOEC)*, 2011.

[2] M. Salsi, C. Koebele, P. Tran, H. Mardoyan, E. Dutisseuil, J. Renaudier, M. Bigot-Astruc, L. Provost, S. Richard, and P. Sillard, "Transmission of 96* 100Gb/s with 23% super-FEC overhead over 11,680 km, using optical spectral engineering," in *Proc. Opt. Fiber Comm. Conf. (OFC/NFOEC)*, 2011.

[3] D. Foursa, Y. Cai, J. Cai, C. Davidson, O. Sinkin, W. Anderson, A. Lucero, A. Pilipetskii, G. Mohs, and N. Bergano, "Coherent 40 gb/s transmission with high spectral efficiency over transpacific distance," in *Proc. Opt. Fiber Comm. Conf. (OFC/NFOEC)*, 2011.

[4] M. Huang, Y. Huang, E. Ip, Y. Shao, and T. Wang, "WDM transmission of 152-gb/s polarization multiplexed RZ-16QAM signals with 25-GHz channel spacing over 15x80-km of SSMF," in *Proc. Opt. Fiber Comm. Conf. (OFC/NFOEC)*, 2011.

[5] X. Zhou, L. Nelson, P. Magill, R. Isaac, B. Zhu, D. Peckham, P. Borel, and K. Carlson, "PDM-nyquist-32QAM for 450-gb/s per-channel WDM transmission on the 50 GHz ITU-t grid," *Journal of Lightwave Technology*, vol. 30, no. 4, pp. 553–559, 2012.

[6] T. Sugihara, T. Kobayashi, T. Fujimori, and T. Mizuochi, "Electronic pre-equalization technologies using high-speed DAC," in *Proc. Europ. Conf. Opt. Comm. (ECOC)*, 2011.

[7] S. Yamanaka, T. Kobayashi, A. Sano, H. Masuda, E. Yoshida, Y. Miyamoto, T. Nakagawa, M. Nagatani, and H. Nosaka, "11 x 171 gb/s PDM 16-QAM transmission over 1440 km with a spectral efficiency of 6.4 b/s/hz using high-speed DAC," in *Proc. Europ. Conf. Opt. Comm. (ECOC)*, 2010.

[8] J.-X. Cai, Y. Cai, C. Davidson, D. Foursa, A. Lucero, O. Sinkin, W. Patterson, A. Pilipetskii, G. Mohns, and N. Bergano, "Transmission of 96 times 100G pre-filtered PDM-RZ-QPSK channels with 300% spectral efficiency over 10,608 km and 400% spectral efficiency over 4,368 km," in *Proc. Opt. Fiber Comm. Conf. (OFC/NFOEC)*, 2010.

[9] J. Wang, X. He, K. Gao, and L. Myers, "8 times 400-gbit/s PDM-QPSK with 100 GHz channel spacing over 2000km transmission using MAP detection," in *Proc. Conf. Lasers El.-Opt. (CLEO)*, 2011.

[10] J.-X. Cai, Y. Cai, C. Davidson, A. Lucero, H. Zhang, D. Foursa, O. Sinkin, W. Patterson, A. Pilipetskii, G. Mohs, and N. Bergano, "20 tbit/s capacity transmission over 6,890 km," in *Proc. Opt. Fiber Comm. Conf. (OFC/NFOEC)*, 2011.

[11] A. Ghazisaeidi, "Impact of tight optical filtering on the performance of 28 gbaud nyquist-WDM PDM-8QAM over 37.5 GHz grid," in *Proc. Opt. Fiber Comm. Conf. (OFC/NFOEC) (to be presented)*, 2013.

[12] S. Savory, A. Steward, S. Wood, G. Gavioli, M. Taylor, R. Kiley, and P. Bayvel, "Digital equalisation of 40gbit/s per wavelength transmission over 2480km of standard fibre without optical dispersion compensation ECOC 2006," in *Proc. Europ. Conf. Opt. Comm. (ECOC)*, 2006.

[13] A. Neves and C. Panazio, "A class of channels resulting in ill-convergence for CMA in decision feedback equalizers," *Signal Processing, IEEE Transactions on*, vol. 58, no. 11, pp. 5736–5743, 2010.

[14] J. Proakis, *Digital Communications*. New York: McGraw-Hill, 2001.

[15] J. Cai, "100G transoceanic length transmission with high spectral efficiency using bandwidth constrained PDM-QPSK," in *Proc. Opt. Fiber Comm. Conf. (OFC/NFOEC)*, 2011.

[16] M. Alfiad, D. van den Borne, M. Kuschnerov, B. Spinnler, T. Wuth, A. Napoli, S. Jansen, and H. de Waardt, "FFE, DFE and MLSE equalizers in phase modulated transmission systems," in *LEOS Annual Meeting*. IEEE, 2009, pp. 193–194.

[17] Y. Mori, K. Igarashi, K. Katoh, and K. Kikuchi, "Decision-feedback carrier-phase estimation for digital coherent optical receivers," in *Proc. Aust. Conf. Opt. Fibre Tech. (OECC/ACOFT)*, 2008.

[18] X. Zhang, X. Pang, L. Deng, D. Zibar, I. Monroy, and R. Younce, "High phase noise tolerant pilot-tone-aided DP-QPSK optical communication systems," *Optics Express*, vol. 20, no. 18, pp. 19 990–19 995, 2012.

[19] A. Liavas, "On the robustness of the finite-length MMSE-DFE with respect to channel and second-order statistics estimation errors," *Signal Processing, IEEE Transactions on*, vol. 50, no. 11, pp. 2866–2874, 2002.

[20] M. Miyoshi and Y. Kaneda, "Inverse filtering of room acoustics," *Acoustics, Speech and Signal Processing, IEEE Transactions on*, vol. 36, no. 2, pp. 145–152, 1988.

[21] G. Strang, *Introduction to linear algebra*. Wellesley Cambridge Pr, 2003.

[22] J.-X. Cai, Y. Cai, Y. Sun, C. Davidson, D. Foursa, A. Lucero, O. Sinkin, W. Patterson, A. Pilipetskii, G. Mohns, and N. Bergano, "112 times 112 gb/s transmission over 9,360 km with channel spacing set to the baud rate (360% spectral efficiency)," in *ECOC*, 2010.

[23] R. Paschotta, A. Schlatter, S. Zeller, H. Telle, and U. Keller, "Optical phase noise and carrier-envelope offset noise of mode-locked lasers," *Applied Physics B*, vol. 82, no. 2, pp. 265–273, 2006.
[24] A. Viterbi and A. Viterbi, "Nonlinear estimation of psk-modulated carrier phase with ap- plication to burst digital transmission," *IEEE Trans. on Information Theory*, vol. 19, no. 4, pp. 543–551, 1983.

ACKNOWLEDGMENTS

This work was partially funded by the Belgian FNRS (Fonds National de la Recherche Scientifique). The authors thank S. Bigo for useful comments and discussions.

Jessica Fickers received the B.S. degree in electrical engineering, and the M.S. degree in physical engineering, both from the Université libre de Bruxelles, Belgium. She is currently working towards the Ph.D. degree in electrical engineering at Université libre de Bruxelles. Her research interests include optical fiber communications, wireless communications and digital signal processing.

Amirhossein Ghazisaeidi received the B.S. degree in electrical engineering, and the M.S. degree in telecommunications systems, both from the electrical engineering department of Sharif University of Technology, Tehran, Iran. He received the Ph.D. degree from the Center for optics photonics, and laser (COPL), ECE department, Université Laval, Quebec City, QC, Canada. He was a postdoctoral researcher in COPL from October 2010 up to June 2011. In July 2011 he joined Alcatel-Lucent Bell-Labs at Villarceaux, Nozay, France, where he is doing research on signal processing algorithms for optical transmission systems. His research interests include signal processing for optical transceivers, performance analysis of optical links, dynamics and noise properties of optical amplifiers, and modeling optoelectronic devices.

Massimiliano Salsi (M'03) was born in Parma, Italy, in 1979. He obtained his Laurea degree in telecommunication engineering (cum laude) and his Ph.D. in information technology in 2004 and 2008 respectively, from the University of Parma, Parma, Italy. He is a Member of Technical Staff in Bell Labs Optical Network research domain in France since 2008. His current research interests are long-haul submarine transmission systems, digital signal processing algorithms for optical coherent detection and mode division multiplexing on few-mode optical fibers. Dr. Salsi has authored or co-authored more than 60 papers and 12 patent applications. He served as technical committee member for the IEEE Summer Topicals Meeting 2012.

Gabriel Charlet received an engineering degree from the Ecole Supérieure dÓptique in 1999 (Orsay, France) and a Ph.D. in physics in 2011 from University Paris XI. He joined Alcatel Research and Innovation (now Alcatel Lucent Bell Labs France) in 2000. Since then he has been working on WDM transmission systems and realized several multi-terabit/s transmission records. He also addressed the topic of advanced modulation formats. He is the author of 10 Postdeadline papers in major conferences and more than 30 patents. In 2007, he received the Fabry de Gramont award for its work on fiber optics communication. In 2010, he has been selected by the Technology Review from MIT as one the 35 innovators below 35 years for its work on 100 Gbit/s and coherent detection. In 2011, he has been selected by Fast Compagny as one of the 100 most creative people in business.

Philippe Emplit (M'94) received the M.S. degree in physics from the Université libre de Bruxelles, Belgium, in 1981. He received the Dr.Sc. degree (with honors) from the same university in 1992. In 1981, he joined, as a doctoral fellow, the Service OPERA of the Ecole polytechnique de Bruxelles, the engineering Faculty of the Université libre de Bruxelles, where he obtained a position of Research Assistant in 1984. He joined the academic staff of the university in 1994. His current research interests are nonlinear guided wave photonics, ultrafast phenomena, and their applications to optical communications. He is the author of one book chapter and 60 international scientific publications. Pr. Emplit is presently Vice-rector of his university, in charge of teaching and learning activities. He is a member of IEEE Photonics Society.

François Horlin received the electrical engineering degree and the Ph.D. degree from the Université catholique de Louvain, Louvain-la-Neuve, Belgium, in 1998 and 2002 respectively. In September 2002, he joined the Inter-university Micro-Electronic Center (IMEC), Leuven, Belgium. He lead a project aiming at developing a 4G mobile wireless communication system in collaboration with Samsung Korea. He was also globally responsible for the digital signal processing activity for wireless communications, and was in charge of the coaching of the Ph.D. team and of the definition of the group long term strategy in the field. Since Januray 2007, François Horlin is associate professor at the Université libre de Bruxelles. He is currently giving 3 lectures in the field of digital telecommunications. He is author of a book, author of a book chapter, co-author of two patents, author or coauthor of more than 150 publications in international journals or conferences.